Strain-induced polarization enhancement in $BaTiO_3$ core-shell nanoparticles

Eugene A. Eliseev,[1] Anna N. Morozovska,[2,*] Sergei V. Kalinin,[3,†] and Dean R. Evans[4,‡]

[1]*Frantsevich Institute for Problems of Materials Science, National Academy of Sciences of Ukraine, Omeliana Pritsaka 3, 03142 Kyiv, Ukraine*

[2]*Institute of Physics, National Academy of Sciences of Ukraine, 46, pr. Nauky, 03028 Kyiv, Ukraine*

[3]*Department of Materials Science and Engineering, University of Tennessee, Knoxville, Tennessee 37996, USA*

[4]*Air Force Research Laboratory, Materials and Manufacturing Directorate, Wright-Patterson Air Force Base, Ohio 45433, USA*

(Received 30 August 2023; revised 6 November 2023; accepted 2 January 2024; published 18 January 2024)

Despite fascinating experimental results, the influence of defects and elastic strains on the physical state of nanosized ferroelectrics is still poorly explored theoretically. One of the unresolved theoretical problems is the analytical description of the strongly enhanced spontaneous polarization, piezoelectric response, and dielectric properties of ferroelectric oxide thin films and core-shell nanoparticles induced by elastic strains and stresses. In particular, the 10-nm quasi-spherical $BaTiO_3$ core-shell nanoparticles reveal a giant spontaneous polarization up to 130 $\mu C/cm^2$, where the physical origin is a large Ti off-centering. The available theoretical description cannot explain the giant spontaneous polarization observed in these spherical nanoparticles. This work analyzes polar properties of $BaTiO_3$ core-shell spherical nanoparticles using the Landau-Ginzburg-Devonshire approach, which considers the nonlinear electrostriction coupling and large Vegard strains in the shell. We reveal that a spontaneous polarization greater than 50 $\mu C/cm^2$ can be stable in a (10–100)-nm $BaTiO_3$ core at room temperature, where a 5-nm paraelectric shell is stretched by (3–6)% due to Vegard strains, which contribute to the elastic mismatch at the core-shell interface. The polarization value 50 $\mu C/cm^2$ corresponds to high tetragonality ratios (1.02–1.04), which is further increased up to 100 $\mu C/cm^2$ by higher Vegard strains and/or intrinsic surface stresses leading to unphysically high tetragonality ratios (1.08–1.16). The nonlinear electrostriction coupling and the elastic mismatch at the core-shell interface are key physical factors of the spontaneous polarization enhancement in the core. Doping with the highly polarized core-shell nanoparticles can be useful in optoelectronics and nonlinear optics to increase beam coupling efficiency, electric field enhancement, reduced switching voltages, ionic contamination elimination, catalysis, and electrocaloric nanocoolers.

DOI: 10.1103/PhysRevB.109.014104

I. INTRODUCTION

Despite fascinating experimental results, the influence of size and screening effects, defects, and elastic strains on the physical state of nanosized ferroelectrics is poorly explored theoretically. This precludes the fundamental understanding of underlying physical mechanisms and significantly limits practical applications of these nanomaterials [1,2]. One of the unresolved theoretical problems is the analytical description of the strongly enhanced spontaneous polarization, piezoelectric response, and dielectric properties of ferroelectric oxide thin films [3,4] and core-shell nanoparticles [5–7] induced by elastic strains (e.g., by strains created by a pure lattice mismatch) and/or stresses created by injected elastic defects (e.g., Vegard strains). A solution to this problem would allow one to achieve significant progress in advanced applications of these nanosized ferroelectrics.

Highly enhanced ferroelectricity can be reached in $(Hf, Zr)O_2$ thin films by light-ion bombardment [3]. Due to the ion bombardment, the massive formation of oxygen vacancies appears in the film. These vacancies form elastic dipoles which, due to the mechanism of electrostriction, enhance the spontaneous electric polarization and local piezoelectric response of the film. In a similar way, oxygen-vacancy injection is a pathway to a strong enhancement of the electromechanical response in $BaTiO_3$ thin films [4]. The electromigration and diffusion of the oxygen vacancies, which are elastic dipoles, can induce relatively strong mechanical stresses in ABO_3-type perovskites (so-called Vegard effect) [8,9] and Fe centers recharging in photorefractive oxide ferroelectrics [10]. Due to the electrostriction coupling, the Vegard effect increases the temperature of the paraelectric-ferroelectric phase transition up to 440 K, which is significantly higher than the bulk transition temperature, $T_C = 391$ K. The tetragonality ratio, c/a, increases up to 1.032 near the film surface and decreases to the bulk value ($c/a = 1.011$) only at a distance of 20 lattice constants from the surface. The local piezoelectric response increases a factor of 4 at room temperature. Since the local piezoelectric response is regarded to be proportional to the ferroelectric polarization, it can reach 100 $\mu C/cm^2$ at 300 K in the $BaTiO_3$ thin films [4].

A decade earlier, Zhu *et al.* [5] observed a sharp increase of the c/a ratio up to 1.055 in (5–10)-nm $BaTiO_3$ nanospheres (i.e., no shell) synthesized using solvothermal methods (in comparison with $c/a \approx 1.002$ in 20-nm nanospheres) at 293 K. They concluded the appearance of a reentrant tetragonal phase for particle sizes less than 20 nm was due to competition of shear and compressive stresses on the particle surface.

*Corresponding author: anna.n.morozovska@gmail.com
†Corresponding author: sergei2@utk.edu
‡Corresponding author: dean.evans@afrl.af.mil

The 10-nm quasi-spherical $BaTiO_3$ core-shell nanoparticles reveal a giant spontaneous polarization up to 130 $\mu C/cm^2$ at room temperature, which is five times greater than the bulk value 26 $\mu C/cm^2$ (see Refs. [6,11,12], and references therein). The incorporation of these nanoparticles can have multiple benefits in various applications, such as enhanced beam coupling efficiency [13], reduced switching voltages/DC bias [14,15], ionic contamination elimination [16], and catalysis [17]. Experimental realizations of quasi-spherical $BaTiO_3$ ferroelectric nanoparticles are abundant, and the sizes of (5–50) nm are typical experimental values [18–21]. The nanoparticles embedded in heptane and oleic acid produce core-shell nanoparticles, where the oleic acid is transformed into an organic crystalline (metal carboxylate) shell surrounding the inorganic $BaTiO_3$ core resulting from mechanochemical synthesis during the ball-milling process [22]. The metal carboxylate coating/shell around the $BaTiO_3$ core can be in two forms: one is crystalline and provides a lattice mismatch at the core-shell interface, and the other is noncrystalline without mismatch conditions [6]. The observed polarization enhancement is possible for the $BaTiO_3$ core with the crystalline shell.

It is worth noting that ferroelectric nanoparticles with such giant spontaneous polarization values are not always achievable from the ball-milled mixture without additional processing. Typically, the harvesting technique described in Ref. [23] is required, which relies on an electric field gradient to selectively harvest ferroelectric nanoparticles with the strongest dipole moments from bulk nanoparticle ball-milled mixtures. The total nanoparticle yield of strong dipoles using the ball-milling/mechanochemical synthesis technique has varied from nearly 0% to ∼100% [23], while the harvesting technique has shown to repeatedly provide 100% usable strong dipoles from these mixtures. The harvesting technique was described by Reznikov in Ref. [24] as being a "breakthrough" in solving the problem of irreproducibility. Alternatively, a process of separation via centrifuge or simple sedimentation, where larger particles drop and form agglomerates and small particles remain in suspension, has also shown to provide strong dipoles. Although this latter method has provided the strong dipole particles used in Refs. [6,7], its effectiveness and reliability compared to the proven harvesting technique has not been determined.

The physical origin of the giant spontaneous polarization in the quasi-spherical $BaTiO_3$ core-shell nanoparticles remained a mystery for a long time, until recent x-ray spectroscopic measurements [7] revealed a large Ti-cation off-centering in 10-nm nanoparticles near 300 K confirmed by the tetragonality ratio $c/a \approx 1.0108$ (in comparison with $c/a \approx 1.0075$ for 50-nm nanoparticles). The off-centering of Ti cations is a key factor in producing the enhanced spontaneous polarization in the nanoparticles. Sharp crystalline-type peaks in the barium oleate Raman spectra suggest that this component in the composite core-shell matrix, a product of mechanochemical synthesis, stabilizes an enhanced polar structural phase of the $BaTiO_3$ core.

To the best of our knowledge, there is no available theoretical description that can explain the giant spontaneous polarization repeatedly observed in the $BaTiO_3$ core-shell nanoparticles. Indeed, the surface bond contraction mechanism can only decrease the polarization of the ferroelectric ABO_3-type perovskite nanoparticles [25,26]. Some theoretical papers [27–29] predict the enhancement of a reversible spontaneous polarization in prolate nanoellipsoids, nanorods, and nanowires of ABO_3-type perovskites, when their polarization is directed along the longest axis. A significant polarization enhancement can also appear in nanorods due to the high positive surface tension coefficient and negative linear electrostriction coupling coefficients Q_{12}; the dependence of the Curie temperature on the particle radius R is proportional to the positive value $-\frac{4\mu}{R}Q_{12}$ (see, e.g., Table I in Ref. [30]). Furthermore, this same mechanism leads to a significant reduction of the Curie temperature T_C and spontaneous polarization in spherical $BaTiO_3$ nanoparticles specifically, because the value $-\frac{2\mu}{R}(2Q_{12}+Q_{11})$ is negative, since the condition $\mu > 0$ is required for the surface equilibrium and $2Q_{12}+Q_{11} > 0$ for $BaTiO_3$. The flexo-chemical effect [31] emerging from the joint action of the Vegard stresses and flexoelectric effect, can increase T_C, spontaneous polarization, and c/a in ultrasmall (5 nm or less) spherical $BaTiO_3$ nanoparticles and explain experimental results [5], although the effect rapidly disappears with a radius increase ($\sim\frac{1}{R^2}$) and requires very high values of the flexoelectric coupling and intrinsic strains. The Vegard strains (w_{ij}^s) can significantly increase T_C in spherical $KTa_{1-x}Nb_xO_3$ nanoparticles with $R < 30$ nm [30], as well as in the $BaTiO_3$ core-shell nanoparticles with $R < 10$ nm (see Fig. 9 in Ref. [32]); however, the influence of strong Vegard strains (i.e., w_{ij}^s, >0.5%) on the $BaTiO_3$ spontaneous polarization was not studied in Ref. [32]. Nonlinear electrostriction coupling, which needs to be considered for strains higher than 1%, induces an instability of the sixth-order $BaTiO_3$ thermodynamic potential, because a higher strain changes the positive sign of the sixth-order polarization term at temperatures well below 350 K. Note, the nonlinear electrostriction coupling can be very important for a correct description of polar properties of strained ferroelectric thin films [33,34] and core-shell nanoparticles [35,36].

All aforementioned and many other theoretical works considering $BaTiO_3$ nanoparticles are based on the Landau-Ginzburg-Devonshire (LGD) phenomenological approach, which includes the second, fourth, and sixth powers of polarization in the LGD free energy expansion and only considers linear electrostriction coupling (see, e.g., Ref. [32], and references therein). This work analyzes the polar properties of core-shell $BaTiO_3$ nanoparticles using the LGD free energy functional proposed by Wang *et al.* [37], which includes the eighth power of polarization, and thus allows high Vegard strains in the shell and the nonlinear electrostriction coupling in the core to be considered.

II. PROBLEM FORMULATION, MAIN ASSUMPTIONS, AND CALCULATION DETAILS

A. The problem formulation and main assumptions

Let us consider a spherical $BaTiO_3$ core-shell nanoparticle in the tetragonal phase, whose core of radius R_c is assumed to be a single domain with a spontaneous polarization $\vec{P}_s$ directed along one of the crystallographic directions (e.g., along the polar axis X_3). The crystalline core has a perfect structure (without any defects) and is considered to be insu-

lating (without any free charges). The core is covered with a crystalline shell of thickness ΔR and outer radius R_s. The shell is assumed to be semiconducting and paraelectric due to the high concentration of free charges and elastic defects. We assume that the effective screening length in the shell, λ, is small (less than 1 nm), and thus the free charges provide an effective screening of the core spontaneous polarization and prevent domain formation, so that the assumption of a single-domain core is self-consistent.

We also assume that the elastic defects induce strong Vegard strains, w_{ij}^s, which are regarded as cubic, $w_{ij}^s = \delta_{ij} w_s$, where δ_{ij} is the Kronecker-delta symbol and w_s is the magnitude of Vegard strains in the shell. Actually, typical values of Vegard strains, which originated in perovskite thin films and nanoparticles from, e.g., oxygen vacancies and/or other point defects, are proportional by the product of the defect concentration, c. The defect concentration can exceed (5–10)% near the surface in accordance with many experiments [38–41]. The elastic dipole value, which is determined by the Vegard strain tensor V_s, has a magnitude of $\sim 10^{-29}$ m^{-3} or more [8]. Thus, for high concentrations of the surface defects the Vegard strain amplitude in the shell can be estimated as $|w_s| = V_s c \geqslant 0.05$, since the atomic concentration is about 10^{29} m^{-3}. In accordance with recent experimental results for $BaTiO_3$ thin films with injected oxygen vacancies [4], the creation of a vacancy concentration as high as (5–7.5) at. % is quite possible. That is why the range of Vegard strains is taken from -6% to 6% in this work.

These strains can stress the core due to the elastic mismatch at the core-shell interface. The relative dielectric permittivity tensor of the shell, ε_{ij}^s, is regarded as cubic, $\varepsilon_{ij}^s = \delta_{ij}\varepsilon_s$, and can be very high ($10^2$–$10^3$) as anticipated for the paraelectric state. The core-shell nanoparticle is placed in a dielectric medium (polymer, gas, liquid, air, or vacuum) with an effective dielectric permittivity, ε_e. The core background [42] dielectric permittivity is ε_b. The core-shell geometry is shown in Fig. 1(a).

Below we neglect the contribution of the surface tension, also called an "intrinsic surface stress" [43], which is equal to $-\frac{2\mu}{R_c}$ [27–29]. This contribution can be neglected because it cannot add more than 0.25% to the total strain of the $BaTiO_3$ core. Indeed, the curvature-induced strain $-\frac{2\mu}{R}(2s_{12} + s_{11}) \leqslant 0.0024$ for $R_c \geqslant 5$ nm, elastic compliances combination $2s_{12} + s_{11} = 2.9 \times 10^{-12}$ Pa^{-1}, and $|\mu| \cong$ (1–2) N/m [44,45].

The LGD free energy density includes the Landau-Devonshire expansion in even powers of the polarization P_3 (up to the eighth power), the Ginzburg gradient energy, and the elastic and electrostriction energies, which are listed in Sec. A 1 of the Supplemental Material [46] and Refs. [47–50] therein. The equilibrium polarization distribution in the core follows from the Euler-Lagrange equation, which in turn follows from the minimization of the LGD free energy, and has the form

$$[\alpha - 2\sigma_i(Q_{i3} + W_{ij3}\sigma_j)]P_3 + (\beta - 4Z_{i33}\sigma_i)P_3^3 + \gamma P_3^5 + \delta P_3^7 - g_{33kl}\frac{\partial^2 P_3}{\partial x_k \partial x_l} = E_3. \quad (1)$$

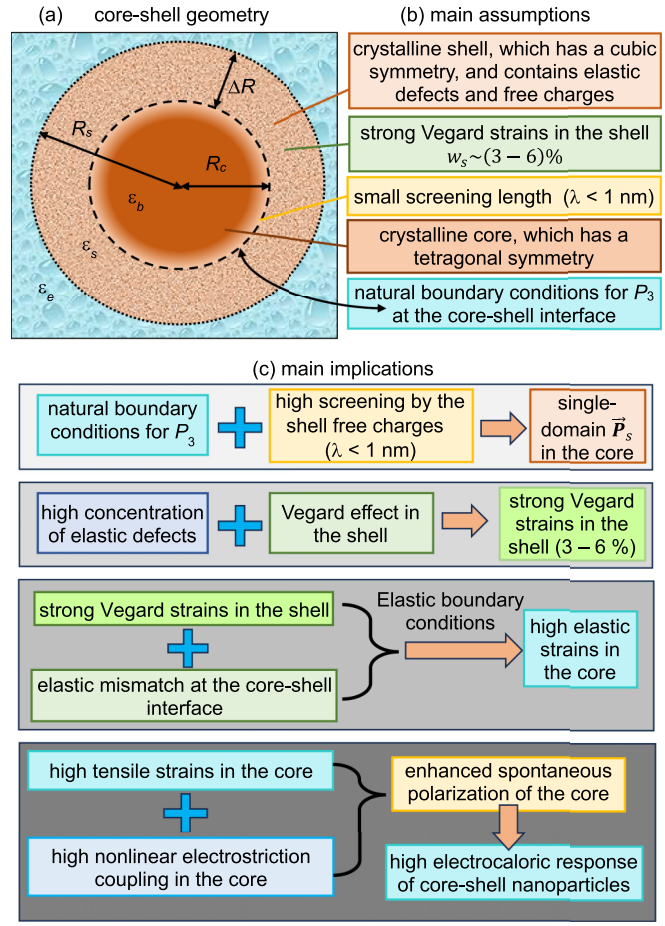

FIG. 1. (a) A spherical core-shell nanoparticle: a ferroelectric core of radius R_c is covered with a paraelectric shell of thickness ΔR, which is full of elastic defects and free charges. The nanoparticle is placed in an isotropic dielectric medium; ε_b, ε_s, and ε_e are the core background, shell, and surrounding media dielectric permittivities. (b),(c) Block scheme of the main assumptions (b) and their implications (c).

Here the parameters α, β, γ, and δ are the second-, fourth-, sixth-, and eighth-order Landau expansion coefficients in the P_3 powers of the free energy corresponding to the bulk $BaTiO_3$. The values σ_i denote diagonal components of a stress tensor in Voigt notation, and subscripts i, j = 1–6. The values Q_{i3}, Z_{i33}, and W_{ij3} are the components of a single linear and two nonlinear electrostriction strain tensors in Voigt notation, respectively [51,52]. The values g_{33kl} are polarization gradient coefficients in matrix notation, and subscripts k, l = 1–3.

The boundary conditions to Eq. (1) determine the long-range and the short-range contributions [53] to the polarization behavior. The LGD approach considers the contribution of the long-range depolarization field, which is determined by the effective screening length λ at the core-shell interface, and the short-range surface energy contribution to the polarization, which is determined by the extrapolation length [54]. The general form of the polarization boundary conditions is $g_{33ij}n_i(\frac{\partial P_3}{\partial x_j} - \frac{P_3}{\Lambda_j}) = 0$, where extrapolation lengths Λ_j can be positive, zero, or negative. Despite the values of Λ_j are poorly known, their influence on the polarization is significant only in

the immediate vicinity of the core surface (one to three lattice constants) [53]. That is why below we analyze the results for the case of infinite extrapolation length, which corresponds to the Neumann boundary conditions at the nanoparticle surface S, $g_{33kl}n_k\frac{\partial P_3}{\partial x_l}|_S = 0$, where $\vec{n}$ is the outer normal to the surface. These conditions are also called "natural" because corresponding surface energy is zero in this case. Only the natural boundary conditions are consistent with the assumption of the constant single-domain P_3, which in turn allows simple analytical expressions for the phase transition temperature, spontaneous polarization, and electrocaloric response studied in this work.

The value E_3 is an electric field component, collinear with the polarization P_3, which is a superposition of external and depolarization fields, E_3^0 and E_3^d, respectively. The quasi-static field E_3 is related to the electric potential φ as $E_3 = -\frac{\partial\varphi}{\partial x_3}$. The potential φ satisfies the Poisson equation inside the particle core, the Debye equation in the semiconducting shell, and the Laplace equation outside the screening shell (see Supplemental Material Sec. A 1 for details).

The parameters of the $BaTiO_3$ core and paraelectric shell used in our calculations are listed in Supplemental Material Tables AI and AII in Supplemental Material Sec. A 1 [46], respectively. In order to focus on the influence of linear and nonlinear electrostriction effects, we do not consider the surface tension and flexoelectric coupling in this work. The scalar parameters α, β, γ, and δ in Eq. (1) are related with tensorial coefficients, a_i, a_{ij}, a_{ijk}, and a_{ijkl} in the LGD free energy (A.2) from Supplemental Material Sec. A 1 [46] in a conventional way. Namely, $\alpha = 2a_1$, $\beta = 4a_{11}$, $\gamma = 6a_{111}$, and $\delta = 8a_{1111}$ in the tetragonal phase of the core. In what follows, we consider two sets of the $BaTiO_3$ core parameters taken from Wang *et al.* [37]:

(1) A widely used "2–4–6 LGD" free energy functional, which includes the second, fourth, and sixth powers of the polarization P_3 in the Landau-Devonshire free energy with the nonlinear electrostriction coupling tensors set to zero, $Z_{ijk} = 0$, $W_{ijk} = 0$ (see the second column in Supplemental Material Table AI). The coefficient α depends linearly on the temperature T, $\alpha(T) = \alpha_T(T - T_C)$, where $T_C = 381$ K is the Curie temperature. Also, the coefficients β and γ linearly depend on the temperature and can change their sign. Since $\delta = 0$, the 2–4–6 LGD functional becomes unstable above 445 K, when γ becomes negative. This is very inconvenient for the modeling of strongly stressed nanoparticles, because elastic stresses above 1% can reduce the instability temperature (room or lower), making the 2–4–6 LGD free energy functional unsuitable for the modeling of strongly stressed nanoparticles.

(2) A more rarely used functional is the "2–4–6–8 LGD" free energy functional, which includes the second, fourth, sixth, and eighth powers of the polarization P_3 in the Landau-Devonshire free energy without consideration of the nonlinear electrostriction coupling effect, i.e., $Z_{ijk} = 0$ and $W_{ijk} = 0$ (see the third column in Supplemental Material Table AI). For this case, the coefficient α also depends linearly on the temperature T, $\alpha(T) = \alpha_T(T - T_C)$, where $T_C = 391$ K. The coefficients β and γ linearly depend on the temperature and can change sign, but the coefficient δ is positive and temperature independent. Since $\delta > 0$, the 2–4–6–8 LGD free energy functional is stable for arbitrary temperatures, and thus is suitable for artifact-free modeling of strongly stressed nanoparticles.

The most important part of this work is to study how the nonlinear electrostriction coupling effect ($Z_{ijk} \neq 0$ and $W_{ijk} \neq 0$) influences the stability conditions of the 2–4–6 and 2–4–6–8 LGD free energy functionals and determines the changes in spontaneous polarization that are induced by the nonlinear electrostriction effect. Different sets of electrostriction coefficients Z_{ijk} determined from different experiments [55–65] or *ab initio* calculations [33] are listed in Supplemental Material Table AIII [46]. In accordance with the table, the values of Z_{ijk} can vary from -14.2 to $+0.38\,\mathrm{m}^8/\mathrm{C}^4$ in a bulk $BaTiO_3$; and the "scattering" range is very wide. Since recent works reveal an extraordinarily high electrostriction due to the interface effects [66], we can assume that a possible range of the Z_{ijk} variation can be even wider in the core-shell $BaTiO_3$ nanoparticles. These speculations give us some grounds to vary Z_{ijk} within the range from -1.5 to $+1.5\,\mathrm{m}^8/\mathrm{C}^4$ to look for optimal values that correspond to the highest spontaneous polarization and the best related properties over the full temperature range of the investigation, (0–500) K. The values of W_{ijk} are small having the order of $10^{-12}\,\mathrm{m}^4/(\mathrm{Pa\,C}^2)$ for ferroelectric perovskites [33].

Elastic stresses in the core, σ_i, induced by the Vegard strains in the shell, can be calculated analytically using the method of successive approximations. When the spontaneous polarization is absent in the paraelectric phase of the core, or small in the "shallow" ferroelectric state located near the paraelectric-ferroelectric transition, the core can be considered as elastically isotropic due to its cubic symmetry or very small tetragonality related with the small electrostriction contribution. When searching numerically for the optimal values of W_{ijk} and Z_{ijk} in the core, we also check whether the values are small enough for the validity of the elastically isotropic approximation in the core-shell nanoparticle.

B. Approximate analytical description

For the case of natural boundary conditions used in this work, $g_{33ij}n_i\frac{\partial P_3}{\partial x_j} = 0$, small λ, and relatively large gradient coefficients $|g_{ijkl}| > 10^{-11}\,\mathrm{C}^{-2}\,\mathrm{m}^3$ J, the polarization gradient effects can be neglected in a single-domain state, which reveals a minimal energy in comparison to polydomain states. The field dependence of a quasi-static single-domain polarization can be found from the following equation:

$$\alpha^* P_3 + \beta^* P_3^3 + \gamma P_3^5 + \delta P_3^7 = E_3^e. \tag{2}$$

The depolarization field, E_3^d, and stresses, σ_i, contribute to the "renormalization" of coefficient $\alpha(T)$, which becomes the temperature-, radius-, stress-, and screening length-dependent function α^* [36]:

$$\alpha^*(T, R_c,\ \sigma_i) = \alpha(T) + \frac{1}{\varepsilon_0(\varepsilon_b + 2\varepsilon_s + R_c/\lambda)} - \sigma_i(2Q_{i3} + W_{ij3}\sigma_j). \tag{3a}$$

The derivation of the second term in Eq. (3a) is given in Ref. [67]. Here, $\lambda = \lambda(E_3^d)$ can be a rather small value (less than 0.1–1 nm) due to free charges and surface band bending

in the shell. Resulting from the nonlinear electrostriction coupling, the coefficient β^* is "renormalized" by elastic stresses as

$$\beta^*(\sigma_i) = \beta - 4Z_{i33}\sigma_i. \tag{3b}$$

In the right-hand side of Eq. (2), E_3^e is the static external field inside the core, for which the estimate $E_3^e \approx \frac{3\varepsilon_s E_3^0}{\varepsilon_b+2\varepsilon_s+R_c/\lambda}$ is valid. If $\lambda(E_3^0) \gg R_c$ and $\varepsilon_s \sim \varepsilon_b$, the field in the core is of the same order as the applied field E_3^0 (see details in Ref. [36]).

In Supplemental Material Sec. A 2 [46] an approximate expression for the diagonal stresses in the core and shell is derived. The core stresses, further denoted as σ_i^c, are given by the expression

$$\sigma_1^c = \sigma_2^c = \sigma_3^c = \frac{-2\left(R_s^3 - R_c^3\right)\left(Q_c P_3^2 + Z_c P_3^4 - w_s\right)}{2\left(R_s^3 - R_c^3\right)\left(s_{11}^c + 2s_{12}^c + W_c P_3^2\right) + R_s^3\left(s_{11}^s - s_{12}^s\right) + 2R_c^3\left(s_{11}^s + 2s_{12}^s\right)}. \tag{4a}$$

Here, s_{ij}^c and s_{ij}^s are the elastic compliances of the core and shell, respectively; $Q_c = (Q_{11} + 2Q_{12})/3$, $Z_c = (Z_{111} + 2Z_{211})/3$, and $W_c = (W_{111} + 2W_{112} + 2W_{123} + 4W_{122})/3$ are isotropic parts of the linear and nonlinear electrostriction tensors of the core, and w_s is the Vegard strain in the shell. The electrostriction coupling can exist in the shell; however, it does not contribute to the solution (4a) for small λ, since the electric field is very small in the shell due to the high screening degree. The nondiagonal stresses are absent, $\sigma_4^c = \sigma_5^c = \sigma_6^c = 0$.

The corresponding free energy of the core-shell nanoparticle is

$$G = \left[\alpha + \frac{1}{\varepsilon_0(\varepsilon_b + 2\varepsilon_s + R_c/\lambda)}\right]\frac{P_3^2}{2} + \frac{\beta P_3^4}{4} + \frac{\gamma P_3^6}{6} + \frac{\delta P_3^8}{8} + \frac{3\left(R_s^3 - R_c^3\right)\left(Q_c P_3^2 + Z_c P_3^4 - w_s\right)^2}{2\left(R_s^3 - R_c^3\right)\left(s_{11}^c + 2s_{12}^c + W_c P_3^2\right) + R_s^3\left(s_{11}^s - s_{12}^s\right) + 2R_c^3\left(s_{11}^s + 2s_{12}^s\right)}. \tag{4b}$$

Since inequality $s_{11}^s - 2s_{12}^s > 0$ follows from the mandatory condition of a positive quadratic form of the elastic energy and $R_s^3 - R_c^3 > 0$, the denominators in Eq. (4) are always positive. The expressions (4) are accurate enough to provide a first approximation for the description of the core in a "deep" ferroelectric phase, when the absolute value of the polarization-dependent anisotropic contribution to the total strain is much smaller than other contributions (see Supplemental Material Sec. A 2 for details). The approximation imposes definite conditions on poorly known (or unknown) anisotropic parts of the tensors Z_{ijk} and W_{ijk}. In order to avoid complications, the tensors are regarded as isotropic. The condition $W_c \geqslant 0$ should be valid for the free energy stability at high P_3, and this condition is assumed hereinafter.

If the term $W_c P_3^2$ is small and positive, Eq. (4a) becomes much simpler for two important cases: (1) when elastic compliances of the core and the shell are the same: $s_{ij}^s = s_{ij}^c \equiv s_{ij}$, and (2) for shells with $\Delta R \ll R_c$. In these cases

$$\sigma_1^c = \sigma_2^c = \sigma_3^c \approx \begin{cases} -\frac{2\left(R_s^3 - R_c^3\right)}{3R_s^3}\frac{Q_c P_3^2 + Z_c P_3^4 - w_s}{s_{11}+s_{12}}, & s_{ij}^s = s_{ij}^c \equiv s_{ij}, \\ \frac{\Delta R}{R_s}\frac{1}{s_{11}^s + s_{12}^s}\left(w_s - Q_c P_3^2 - Z_c P_3^4\right), & \Delta R \ll R_c. \end{cases} \tag{5}$$

After substitution of the solution (5) in Eq. (2) and elementary transformations (see Supplemental Material Sec. A 3 for details), the equation for polarization P_3 with renormalized coefficients α_R, β_R, γ_R, δ_R, and ϵ_R is derived as

$$\alpha_R P_3 + \beta_R P_3^3 + \gamma_R P_3^5 + \delta_R P_3^7 + \epsilon_R P_3^9 = E_3^e. \tag{6a}$$

The renormalized coefficients are given by expressions

$$\alpha_R = \alpha + \frac{1}{\varepsilon_0(\varepsilon_b + 2\varepsilon_s + R_c/\lambda)} - 4Q_c\frac{\left(R_s^3 - R_c^3\right)w_s}{R_s^3(s_{11}+s_{12})} + \frac{4}{3}W_c\left(\frac{\left(R_s^3 - R_c^3\right)w_s}{R_s^3(s_{11}+s_{12})}\right)^2, \tag{6b}$$

$$\beta_R = \beta + 6Q_c^2\frac{2\left(R_s^3 - R_c^3\right)}{3R_s^3(s_{11}+s_{12})} - 8Z_c\frac{\left(R_s^3 - R_c^3\right)w_s}{R_s^3(s_{11}+s_{12})} - \frac{8}{3}W_c Q_c w_s\left(\frac{R_s^3 - R_c^3}{R_s^3(s_{11}+s_{12})}\right)^2, \tag{6c}$$

$$\gamma_R = \gamma + \frac{12\left(R_s^3 - R_c^3\right)}{R_s^3(s_{11}+s_{12})}Q_c Z_c + \frac{4}{3}W_c\left(Q_c^2 - 2Z_c w_s\right)\left(\frac{R_s^3 - R_c^3}{R_s^3(s_{11}+s_{12})}\right)^2, \tag{6d}$$

$$\delta_R = \delta + Z_c^2\frac{8\left(R_s^3 - R_c^3\right)}{R_s^3(s_{11}+s_{12})} + \frac{8}{3}W_c Q_c Z_c\left(\frac{R_s^3 - R_c^3}{R_s^3(s_{11}+s_{12})}\right)^2, \tag{6e}$$

$$\epsilon_R = \frac{4}{3}W_c Z_c^2\left(\frac{R_s^3 - R_c^3}{R_s^3(s_{11}+s_{12})}\right)^2. \tag{6f}$$

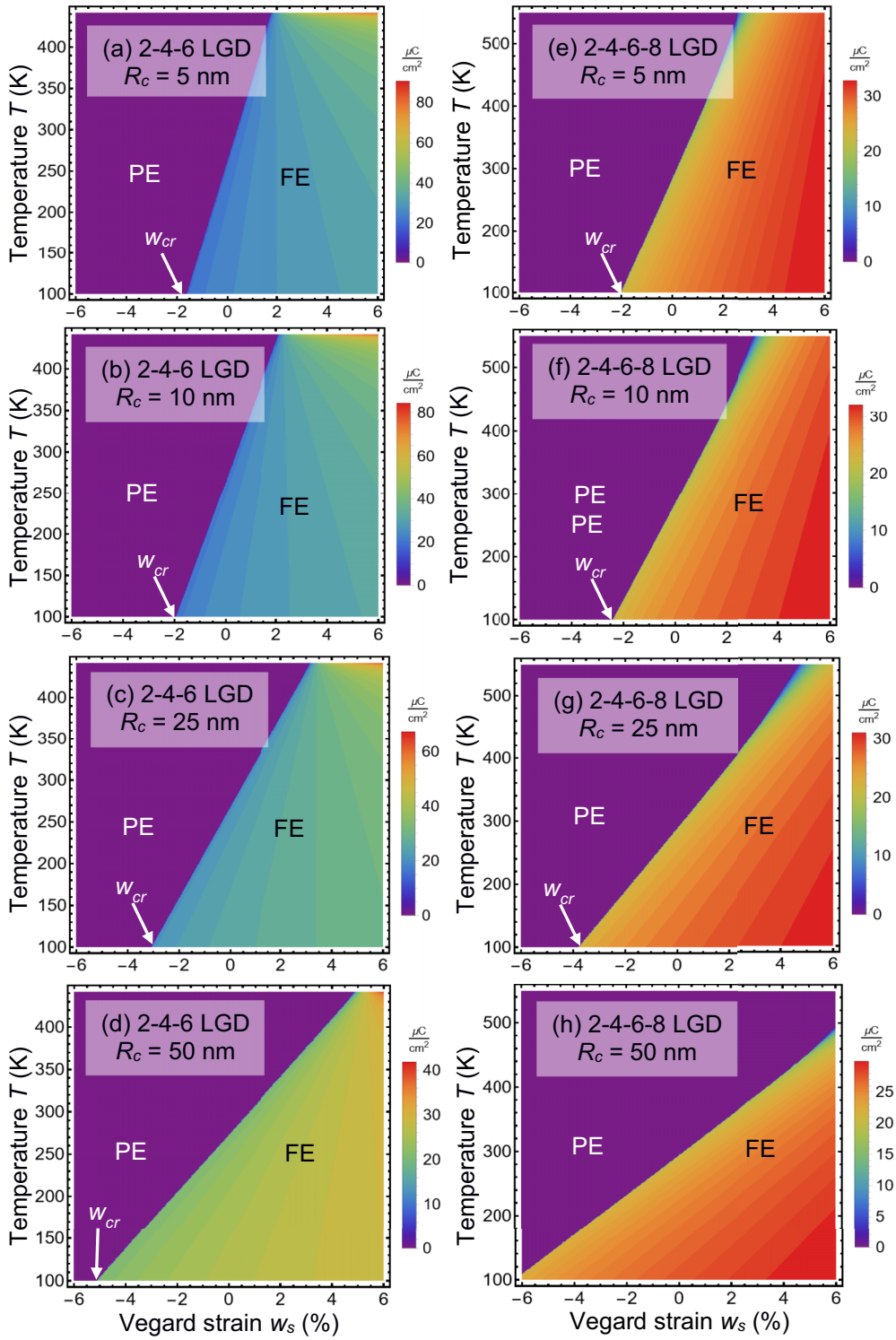

FIG. 2. The spontaneous polarization P_s of a single-domain $BaTiO_3$ core-shell nanoparticle with radius $R_c = 5$ nm (a), (e), 10 nm (b), (f), 25 nm (c), (g), and 50 nm (d), (h) calculated as a function of temperature T and Vegard strain w_s using the 2–4–6 (a)–(d) and 2–4–6–8 (e)–(h) LGD free energy without nonlinear electrostriction coupling, $\lambda = 0.5$ nm, $\Delta R = 5$ nm, and $\varepsilon_s = 500$. Color coding in the diagrams is the absolute value of P_s in the deepest potential well of the LGD free energy. The color scale shows the P_s in $\mu C/cm^2$. The abbreviations "PE" and "FE" refer to the paraelectric and ferroelectric phases, respectively.

The renormalization of the coefficients in Eq. (6) is proportional to the ratio $\frac{R_s^3 - R_c^3}{3R_s^3}$, which is close to $\frac{\Delta R}{R_s}$ for thin shells with $\Delta R \ll R_c$. The renormalization is most significant for small nanoparticles with $\Delta R \sim R_c$; it vanishes for $R_c \to R_s$ and is absent for thin films, where the curvature disappears, R_c and R_s tend to infinity, and their finite difference ΔR becomes the film thickness.

By definition, the tetragonality c/a is proportional to the ratio:

$$\frac{c}{a} = \frac{1+u_3^c}{1+u_1^c}\,, \tag{7a}$$

where u_3^c and u_1^c are the core (denoted by the superscript c) strains written in Voigt notations. Because the core strains are small, $|u_3^c| \ll 1$ and $|u_1^c| \ll 1$, the tetragonality ratio is proportional to their difference, $\frac{c}{a} \approx 1 + u_3^c - u_1^c$. Since the tensors of nonlinear electrostriction coupling are assumed to be isotropic, their contribution to the u_3^c and u_1^c are the same, namely, $u_3^c = C_1 + Q_{11}P_3^2$ and $u_1^c = C_1 + Q_{12}P_3^2$, where the function C_1 is given by Eq. (A.14a) in Supplemental Material Sec. A 2. Therefore, the deviation of the tetragonality ratio from unity is proportional to the anisotropy of linear electrostriction coefficients of the core:

$$\frac{c}{a} \approx 1 + (Q_{11} - Q_{12})P_3^2. \tag{7b}$$

III. RESULTS AND DISCUSSION

The numerical results presented in this section are obtained and visualized in *Mathematica* 13.2 [68]. The calculations are performed for a small screening length ($\lambda = 0.5$ nm), small thickness ($\Delta R = 5$ nm), and high dielectric permittivity ($\varepsilon_s = 500$) of the paraelectric shell. The spontaneous polarization, P_s, of a single-domain $BaTiO_3$ core is calculated for a range of the core radii $R_c = (5\text{–}50)$ nm as a function of both temperature, T, and Vegard strain, w_s, using 2–4–6 and 2–4–6–8 LGD free energies for zero (Fig. 2) and nonzero (Fig. 3) nonlinear electrostriction coupling tensors, Z_{ijk} and W_{ijk}, which have different dimensionalities, and are responsible for the coupling strength of different contributions in the free energy part Eq. (A.2e), namely, $Z_{ijkl}\sigma_{ij}P_kP_lP_mP_n$ and $W_{ijklmn}\sigma_{ij}\sigma_{kl}P_mP_n$.

Since $Q_c > 0$ for $BaTiO_3$, compressive Vegard strains ($w_s < 0$) suppress P_s and can induce the paraelectric (PE) state, while tensile Vegard strains ($w_s > 0$) increase P_s and support the ferroelectric (FE) state in the $BaTiO_3$ core. For tensile Vegard strains, P_s decreases with an increase of the core radius as shown for the range of radii (5–50) nm used in this study. It is seen from the comparison of the parts (a)–(h) in Figs. 2 and 3 that P_s is the largest for $R_c = 5$ nm and the smallest for $R_c = 50$ nm. Note that the color scale in Figs. 2 and 3 ranges from the maximal positive value (red) to the minimal zero value (dark violet).

The spontaneous polarization calculated using the 2–4–6 LGD free energy, where $Z_{ijk} = 0$ and $W_{ijk} = 0$, is shown in Figs. 2(a)–2(d). P_s appears at some critical temperature- and size-dependent strain, denoted as w_{cr}, and monotonically increases with an increase in w_s to 6%. The magnitude of P_s, which corresponds to $T = 293$ K and a maximal strain (w_s) of 6%, does not exceed $35\,\mu C/cm^2$ for $R_c = 5$ nm and $30\,\mu C/cm^2$ for $R_c = 50$ nm. For the case of small radii [5 and 10 nm in Figs. 2(a) and 2(b)], the magnitude of P_s increases up to (80–85) $\mu C/cm^2$ at temperatures above 440 K (see the red region in the top right corner in the left column of Fig. 2), which is much higher than the bulk value for 293 K ($26\,\mu C/cm^2$). Such an increase of P_s is unphysical, because the temperature increase must weaken and eventually destroy the long-range order. The reason for the unphysically large P_s is because the 2–4–6 LGD free energy becomes unstable at temperatures above 440 K, and large tensile Vegard strains shift the instability temperature to lower temperatures; therefore, these large magnitudes of P_s look artificial and disagree with available experimental data. This strongly suggests that calculating the spontaneous polarization using the 2–4–6 LGD free energy is not practical.

The spontaneous polarization calculated using the 2–4–6–8 LGD free energy, where $Z_{ijk} = 0$ and $W_{ijk} = 0$, is shown in Figs. 2(e)–2(h). The magnitude of P_s, which corresponds to $T = 293$ K and maximal $w_s = 6\%$, does not exceed $30\,\mu C/cm^2$ for $R_c = 5$ nm and $25\,\mu C/cm^2$ for $R_c = 50$ nm. The polarization decreases with a temperature increase (e.g., P_s is smaller than $5\,\mu C/cm^2$ for 500 K, $R_c = 25$ nm, and $w_s = 4\%$), which is physical. The polarization increases up to $30\,\mu C/cm^2$ with the temperature decrease to 100 K (see the red region in the bottom right corner in the right column of Fig. 2), which is reasonable because the lowering temperature supports long-range order. Thus, the 2–4–6–8 LGD free energy being stable, can be used for a better description of $BaTiO_3$ core-shell nanoparticles at arbitrary temperatures and high Vegard strains. However, the magnitude of P_s does not exceed $35\,\mu C/cm^2$, which is too small in comparison with the experimentally observed giant values that exceed $120\,\mu C/cm^2$ [6,11].

Next, we study how the nonlinear electrostriction coupling, under the condition $W_c \geqslant 0$, influences the spontaneous polarization of the $BaTiO_3$ core-shell nanoparticles. In this case, the nonlinear electrostriction coupling does not negatively impact the stability of the 2–4–6–8 LGD functional. We searched numerically for optimal values of W_c and Z_c corresponding to the maximal spontaneous polarization over the full temperature range of the investigation, (0–500) K. At the same time, we made sure to keep the values of W_{ijk} and Z_{ijk} small enough for the validity of the condition $|u_i^{c,s}| \ll 1$ in the core-shell nanoparticle. The obtained optimal values are $W_c = 0$ and $Z_c = 0.28\,m^8/C^4$ for the 2–4–6 LGD free energy functional, and $W_c = 1.2 \times 10^{-12}\,m^4/(Pa\,C^2)$ and $Z_c = 0.44\,m^8/C^4$ for the 2–4–6–8 LGD free energy functional.

The spontaneous polarization, P_s, calculated using the 2–4–6 LGD free energy with nonlinear electrostriction coupling, is shown in Figs. 3(a)–3(d). P_s appears at some critical temperature- and size-dependent strain, denoted as w_{cr}, and monotonically increases with an increase in w_s to 6%. The magnitude of P_s reaches $55\,\mu C/cm^2$ for $R_c = 5$ nm and $50\,\mu C/cm^2$ for $R_c = 50$ nm, $T = 293$ K, and $w_s = 6\%$. Note that P_s strongly increases ($>65\,\mu C/cm^2$) with temperature increase above 440 K only for the 2–4–6 LGD model (the red top right corners are present only in the left column of Fig. 3). Thus, the consideration of the coupling between the Vegard strains and nonlinear electrostriction in the 2–4–6 LGD free energy allows P_s to increase more than a factor of 2 in comparison with the bulk value; however, it does not prevent the functional instability at the temperatures higher than 440 K.

The spontaneous polarization P_s calculated using the 2–4–6–8 LGD free energy with nonlinear electrostriction coupling is shown in Figs. 3(e)–3(h). For the 2–4–6–8 LGD model, P_s

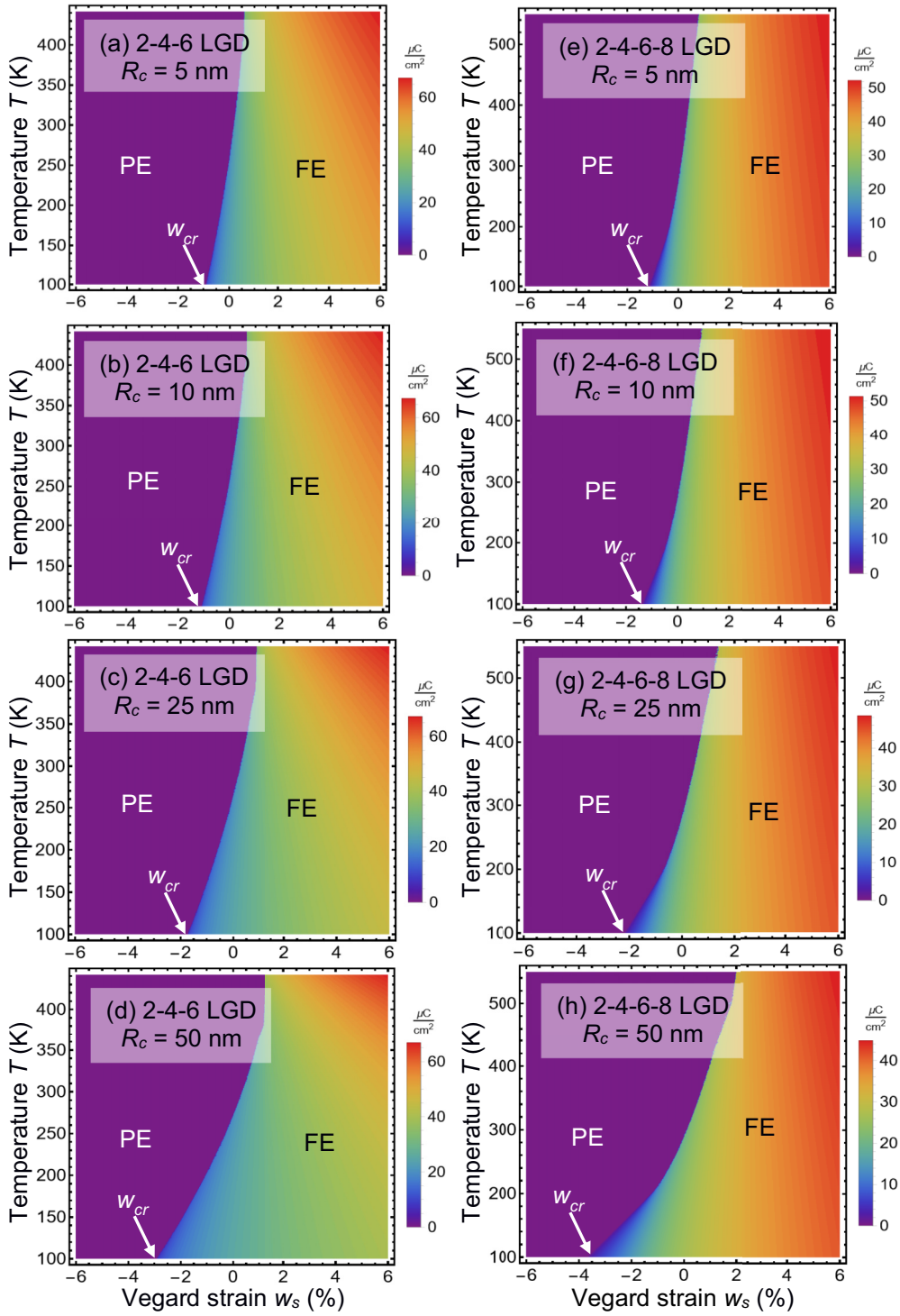

FIG. 3. The spontaneous polarization P_s of a single-domain $BaTiO_3$ core-shell nanoparticle with radius $R_c = 5$ nm (a), (e), 10 nm (b), (f), 25 nm (c), (g), and 50 nm (d), (h) calculated as a function of temperature T and Vegard strain w_s using optimal nonlinear electrostriction values. For 2–4–6 LGD free energy, $W_c = 0$ and $Z_c = 0.27\,\mathrm{m}^8/\mathrm{C}^4$ (a)–(d); and 2–4–6–8 LGD free energy, $W_c = 1.2 \times 10^{-12}\,\mathrm{m}^4/(\mathrm{Pa\,C}^2)$ and $Z_c = 0.44\,\mathrm{m}^8/\mathrm{C}^4$ (e)–(h). Other parameters and designations are the same as in Fig. 2.

increases with a strain increase, and decreases (for $w_s < w_t$) or very slightly increases (for $w_s > w_t$) with the temperature increase. The value of w_t increases from 1.26% for $R_c = 5$ nm to 1.97% for $R_c = 50$ nm [see the black dotted line in Fig. 3(h) and Fig. S1 in Supplemental Material Sec. A 4 [46] for details]. Red depicts high strains in the right column of Fig. 3, and the color gradient changes very weakly as T decreases. Also, P_s decreases with a decrease of w_s and vanishes for w_s close to w_{cr}, which is natural and expected. For $w_s > w_{cr}$ the magnitude of P_s increases with an increase in w_s due to the nonlinear electrostriction coupling. The magnitude of P_s reaches $50\,\mu\mathrm{C/cm}^2$ for $R_c = 5$ nm and $45\,\mu\mathrm{C/cm}^2$ for

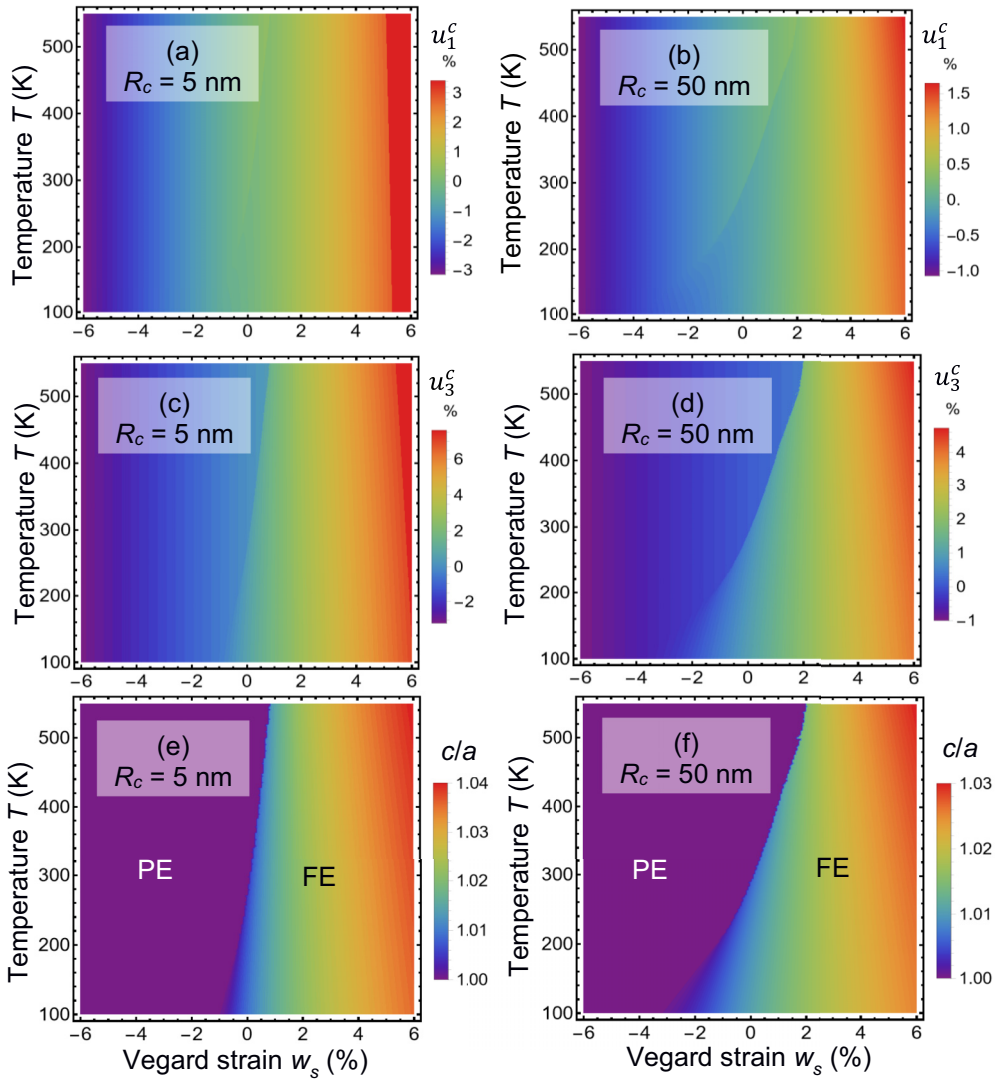

FIG. 4. The strain components u_1^c (a), (b) and u_3^c (c), (d), and the tetragonality ratio c/a (e), (f) of the single-domain $BaTiO_3$ core with radius $R_c = 5$ nm (a), (c), (e) and 50 nm (b), (d), (f) calculated as a function of temperature T and Vegard strain w_s using the 2–4–6–8 LGD free energy; $W_c = 1.2 \times 10^{-12}\,\mathrm{m}^4/(\mathrm{Pa\,C}^2)$ and $Z_c = 0.44\,\mathrm{m}^8/\mathrm{C}^4$. Other parameters are the same as in Fig. 2.

$R_c = 50$ nm at $T = 293$ K and $w_s = 6\%$. Thus, the consideration of the nonlinear electrostriction coupling in the 2–4–6–8 LGD free energy allows P_s to increase a factor of 2 in comparison with the values calculated for 2–4–6–8 LGD free energy with $Z_{ijk} = 0$ and $W_{ijk} = 0$ shown in Figs. 2(e)–2(h). Notably, the calculated slight increase of the spontaneous polarization, which appears with the temperature increase in the strongly tensiled small core-shell nanoparticles considered in the framework of the 2–4–6–8 LGD free energy with a large nonlinear electrostriction coupling, is artifactual (see comments in Supplemental Material Sec. A 4 [46]). Anyway, the maximal values of P_s, which do not exceed $55\,\mu\mathrm{C/cm}^2$, are more than two times smaller in comparison with the experimentally observed values [6,11].

For the plots in Fig. 4, the 2–4–6–8 LGD free energy functional is used with optimal values of W_c and Z_c [i.e., $W_c = 1.2 \times 10^{-12}\,\mathrm{m}^4/(\mathrm{Pa\,C}^2)$ and $Z_c = 0.44\,\mathrm{m}^8/\mathrm{C}^4$]. Note the calculations of the strains and tetragonality ratio using 2–4–6 LGD free energy with optimal values of W_c and Z_c (i.e., $W_c = 0$ and $Z_c = 0.27\,\mathrm{m}^8/\mathrm{C}^4$) give similar results to those shown in Figs. 4(a)–4(d) for the strains u_1^c and u_3^c and in Figs. 4(e) and 4(f) for $\frac{c}{a}$ only at temperatures below 400 K. Note, the strains and tetragonality ratio calculated using 2–4–6 LGD free energy start to increase for temperatures above 400 K, and, in particular, $\frac{c}{a}$ becomes larger than 1.1 when the temperature increases above 440 K. Since $\frac{c}{a} - 1 \approx u_3^c - u_1^c \approx (Q_{11} - Q_{12})P_s^2$ in accordance with Eq. (7), the increase of u_1^c, u_3^c, and $\frac{c}{a}$ for $T > 400$ K is a direct consequence of the spontaneous polarization increase for temperatures $T > 400$ K [as shown in Figs. 3(a)–3(d)]. Since the unphysical increase of P_s^2 happens for $T > 400$ K due to the 2–4–6 LGD free energy inapplicability for temperatures above 440 K, one cannot trust the increase of u_1^c, u_3^c, and $\frac{c}{a}$ for $T > 400$ K, and thus we do not show the figure for the strains and tetragonality ratio calculated using 2–4–6 LGD free energy in this work.

The spontaneous polarization value $50\,\mu\mathrm{C/cm}^2$ corresponds to tensile core strains, u_1^c and u_3^c, as high as (3–6)% [see Figs. 4(a)–4(d)] and tetragonality ratios as high as

1.02–1.04 [see Figs. 4(e) and 4(f)], although this magnitude of the spontaneous polarization is nowhere near the large experimentally measured values. A spontaneous polarization larger than $50\,\mu C/cm^2$ can be reached by the application of higher tensile strains and/or high positive intrinsic surface stresses (note, compressive stains do not contribute to an increase in polarization), however, this would lead to unphysically high tetragonality ratios. In particular, a 27% strain difference (i.e., a tetragonality ratio as high as 1.27) would be required to match the experimentally observed polarization value of $130\,\mu C/cm^2$ [6], which seems physically impossible. This means that physical mechanisms, other than the Vegard and/or mismatch strains, linear and nonlinear electrostriction couplings, which are not considered here, are responsible for the polarization enhancement higher than $100\,\mu C/cm^2$.

As seen from Figs. 2–4, both 2–4–6 and 2–4–6–8 LGD free energies with or without nonlinear electrostriction coupling give less than a half ($\sim 50\,\mu C/cm^2$) of what is experimentally measured for the spontaneous polarization at room temperature ($\sim 100-130\,\mu C/cm^2$). It also should be noted that the polarization of core-shell nanoparticles can depend critically on the preparation method: ball-milled nanoparticles reveal $P_s \cong 130\,\mu C/cm^2$, while much smaller P_s values are measured in nonmilled nanoparticles [6,11]. The discrepancy of more than a factor of 2 between LGD models and experiments [6,11] may be explained by other factors not considered in this work. Below are possible reasons that may explain the discrepancies.

(a) It could be the dependence of the linear electrostriction coefficients Q_{ij} and elastic modulus s_{ij} on the preparation methods of the nanoparticles or post fabrication techniques. Note the effects of nanoparticle preparation on the core-shell interface in Refs. [6,22]; this may be supported by the recent work [66] revealing an extraordinarily high electrostriction due to interface effects.

As a rule, the influence of the interface is important near the surface (i.e., several nanometers from the surface), but the scale may be greater for milled nanoparticles of (5–10)-nm radius having a quasi-cubic or irregular shape, because of their evolved surfaces and corners that contribute to the formation of inhomogeneous internal strains. Note that the elastic mismatch at the core-shell interface and internal strains can also influence the penetration depth of the surface-induced electrostriction: as a rule, the stronger the mismatch and/or strains, the greater the depth can be. Unfortunately, without experimental evidence and/or density functional theory calculations for $BaTiO_3$, quantitative estimates of the interface-induced changes of Q_{ij} magnitude and anisotropy are not reliable. Qualitatively, the several times increase of $|Q_{ij}|$ leads to the several times increase of the Curie temperature shift, $\Delta T_c \sim \frac{2}{\alpha_T} Q_{i3}\sigma_i$, in accordance with Eq. (3a). Furthermore, a change of polarization P_3 is proportional to $\sqrt{T_c + \Delta T_c - T}$, and the tetragonality change is proportional to $(Q_{11}-Q_{12})P_3^2$ in accordance with Eq. (7b). The change can be very strong and reach hundreds of K for ΔT_c [69].

(b) Another explanation may be the following: if the surface tension at the core-shell interface is characterized by a negative coefficient μ, its influence adds to the tensile Vegard and/or mismatch strains and contributes to the total effect of polarization increase. However, in accordance with our estimates made in Sec. II A, the contribution of the surface tension to the strain cannot add more than 0.25%; furthermore, a negative coefficient μ is a very rare case, because the condition $\mu > 0$ is required for the surface equilibrium [70].

(c) Another possibility may be a negative extrapolation length in the boundary conditions for polarization, which would support the surface-induced polarization enhancement. In this case the polarization at the surface can be several times higher than in the bulk [71]. However, the effect of the extrapolation length can be very "short range" [53], meaning that the polarization enhancement induced by the negative extrapolation length would be significant only in a thin subsurface layer, as thin as (3–10) lattice constants.

Below we will show that, due to the polarization enhancement, the Vegard strains can improve the electrocaloric properties of a core-shell ferroelectric nanoparticle, which can be important for applications such as nanocoolers. The relative electrocaloric (EC) temperature change, $\Delta T_{EC} = T_{FE} - T$, can be calculated from the expression [72]

$$\Delta T_{EC} = -T\int_{E_1}^{E_2} \frac{1}{\rho C_P}\left(\frac{\partial P_3}{\partial T}\right)_E dE \approx \frac{T}{\rho C_P}\left(\frac{\alpha_T}{2}\left[P_3^2(E_2)-P_3^2(E_1)\right] + \frac{\beta_T}{4}\left[P_3^4(E_2)-P_3^4(E_1)\right] + \frac{\gamma_T}{6}\left[P_3^6(E_2)-P_3^6(E_1)\right]\right), \tag{8a}$$

where ρ_P is the volume density and C_P is the specific heat of the nanoparticle core; T is the ambient temperature, T_{FE} is the temperature of the ferroelectric core measured in adiabatic conditions; E_1 and E_2 are the values of the quasi-static electric field E_3^e applied to the nanoparticle in adiabatic conditions; and coefficients $\alpha_T = \frac{\partial \alpha_R}{\partial T}$, $\beta_T = \frac{\partial \beta_R}{\partial T}$, and $\gamma_T = \frac{\partial \gamma_R}{\partial T}$ [α_R, β_R, and γ_R are introduced in Eqs. (6)].

Note that we are especially interested in reaching a maximal negative $\Delta T_{EC} < 0$ corresponding to EC cooling of the nanoparticle, which is required for nanocooler-based applications. To reach the maximal $\Delta T_{EC} < 0$, it is necessary to set $E_1 = 0$ and $E_2 = E_c$ in Eq. (8a), where E_c is the coercive field of the core-shell nanoparticle, and determine that the greater polarization corresponds to the larger absolute value of ΔT_{EC}:

$$\Delta T_{EC} \approx -\frac{T}{\rho C_P}\left(\frac{\alpha_T}{2}P_s^2 + \frac{\beta_T}{4}P_s^4 + \frac{\gamma_T}{6}P_s^6\right). \tag{8b}$$

In Eq. (8b), $P_3^2(0) = P_s^2$ and $P_3^2(E_c) = 0$. Since $\alpha_T > 0$, $\beta_T > 0$, and $\gamma_T < 0$ for $BaTiO_3$, the EC effect is negative (cooling, $\Delta T_{EC} < 0$) for small and intermediate values of P_s^2; however, it can change the sign (heating, $\Delta T_{EC} > 0$) for very large values of the spontaneous polarization.

The specific heat depends on polarization for ferroelectrics and can be modeled as follows [73]:

$$C_P = C_P^0 - T\frac{\partial^2 g}{\partial T^2}, \tag{8c}$$

where C_P^0 is the polarization-independent part of specific heat and g is the density of the LGD free energy (A.2) (see Supplemental Material Sec. A 1 [46]). According to

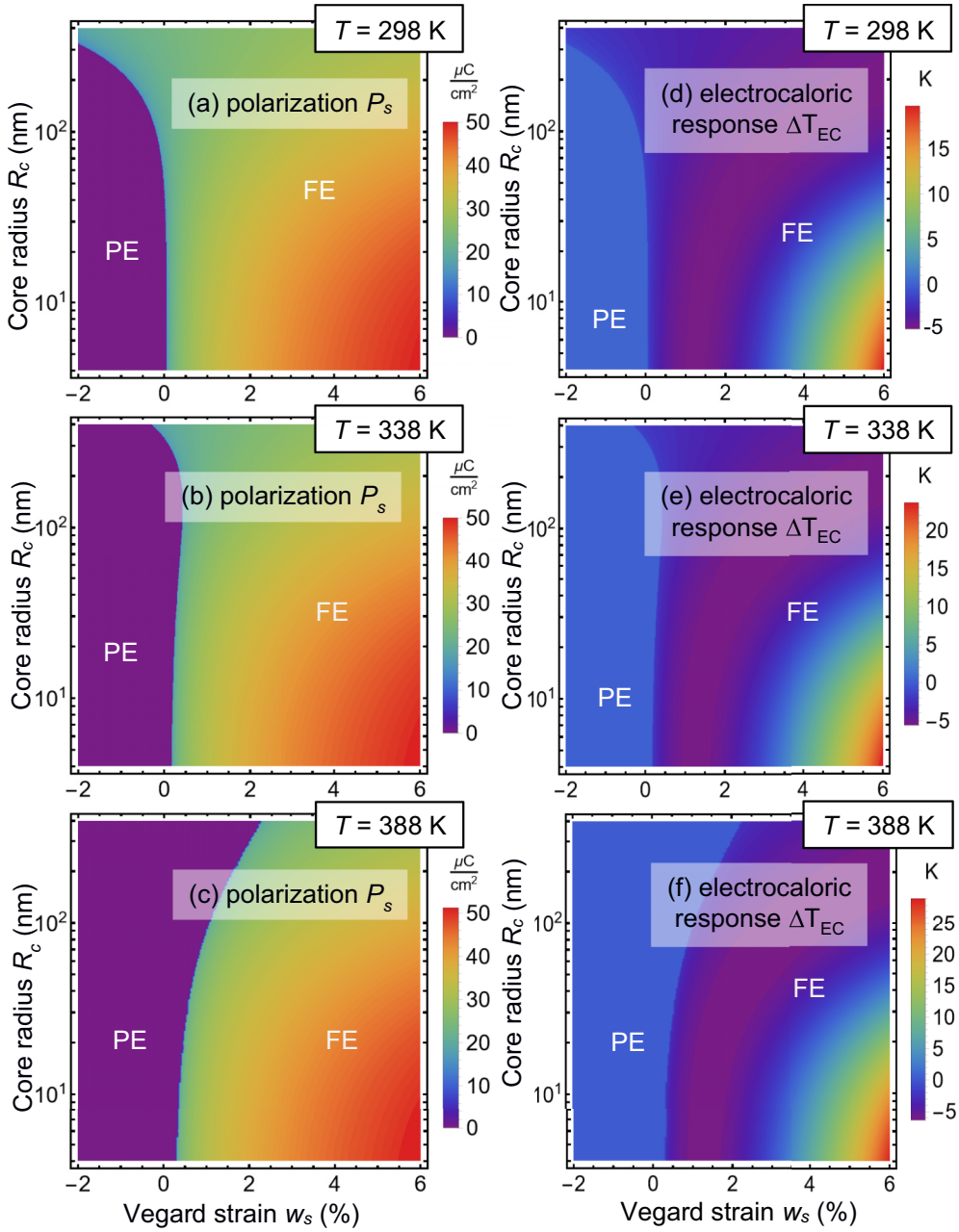

FIG. 5. The spontaneous polarization P_s (a)–(c) and the electrocaloric temperature change ΔT_{EC} (d)–(f) of a single-domain $BaTiO_3$ core-shell nanoparticle calculated as a function of core radius R_c and Vegard strain w_s using the 2–4–6–8 LGD free energy, $W_c = 1.2 \times 10^{-12}\ \mathrm{m^4/(Pa\,C^2)}$ and $Z_c = 0.44\,\mathrm{C^{-4}\ m^8}$, and temperatures $T = 298$ K (a), (d), 338 K (b), (e), and 388 K (c), (f). Color scale corresponds to P_s in $\mu\mathrm{C/cm^2}$ and ΔT_{EC} in K. Other parameters are the same as in Fig. 2.

experimental results, the specific heat usually has a maximum at the point (i.e., coordinates of temperature and radius/strain) of the first-order ferroelectric phase transition, and the maximum height is about (10–30)% of the C_p value near T_C (see, e.g., Ref. [74]). For estimates of the EC temperature change, we assume that the mass density and heat capacitance of the $BaTiO_3$ are $\rho_P = 6.02 \times 10^3\ \mathrm{kg/m^3}$ and $C_P = 4.6 \times 10^2$ J/(kg K), respectively.

The calculations of the EC response are performed over a wide temperature range, (250–400) K; for a range of core radii, $5 < R_c < 50$ nm, for which the Vegard strains are pronounced. The nanoparticle core must be in the ferroelectric state to produce any noticeable EC cooling (e.g., $\Delta T_{EC} < -2$ K); when the core is in the paraelectric state, only a weak EC heating (e.g., $0 < \Delta T_{EC} < 2$ K) is possible [72]. The spontaneous polarization, P_s, and the electrocaloric temperature change, ΔT_{EC}, as a function of the core radius R_c and Vegard strain w_s, are shown in Fig. 5. P_s is calculated for $E_3^e \to 0$, and ΔT_{EC} is calculated for $E_3^e \to E_c$, where E_c is the coercive field. Since $Q_c > 0$, compressive Vegard strains $w_s < 0$ suppress P_s and can induce the PE state, and tensile Vegard strains $w_s > 0$ increase P_s and support the FE state in the $BaTiO_3$ core. Due to the synergy of the size effect and tensile Vegard strain, the

spontaneous polarization reaches (50–30) $\mu C/cm^2$ in the temperature range (298–388) K, which is higher than the corresponding values (26–21) $\mu C/cm^2$ for a bulk $BaTiO_3$. For the same temperature range, the EC cooling of the $BaTiO_3$ core can be more than 6 K from the boundary of the size-induced paraelectric-ferroelectric phase transition. Note that the EC cooling cannot exceed a temperature change of 2.5 K for a bulk $BaTiO_3$ nor for unstrained $BaTiO_3$ nanoparticles in accordance with earlier LGD-based theoretical calculations [72]. The tensile Veard strain increases the spontaneous polarization, which in turn increases the EC temperature change according to Eq. (8b).

The change in the sign of the EC effect with an increase in the spontaneous polarization is related to the features of the LGD free energy for $BaTiO_3$, where not only the coefficient at the second power of polarization depends on temperature, but also the coefficients at the fourth and sixth powers. According to Eq. (8a), this leads to several contributions to the electrocaloric effect, which are proportional to the corresponding polarization powers. Since the coefficient γ_T is negative, the EC effect changes sign for large values of the polarization.

Figure 5 demonstrates the size effect of the spontaneous polarization and electrocaloric response, which becomes especially pronounced for $R_c < 100$ nm. The size effect of the polarization primarily originates from the depolarization field, whose contribution to the Curie temperature is proportional to the expression $\frac{1}{\alpha_T \varepsilon_0(\varepsilon_b+2\varepsilon_s+R_c/\lambda)}$ [see the second term in Eq. (3a)]. A secondary contribution originates from the size dependence of the elastic stress σ_j included in the third term in Eq. (3a), $\sigma_i(2Q_{i3} + W_{ij3}\sigma_j)$. Since the depolarization field contribution is roughly proportional to $\frac{1}{\alpha_T \varepsilon_0}\frac{\lambda}{R_c}$ and σ_j is proportional to $\frac{w_s}{s_{11}+s_{12}}\frac{\Delta R}{R_c}$ for $\Delta R \ll R_c$ in accordance with Eq. (5), the values $\frac{\lambda}{\alpha_T \varepsilon_0}$ and $\frac{w_s \Delta R}{s_{11}+s_{12}}$, and the sign of the Vegard strain w_s determine the rate of the power decay $\sim \frac{1}{R_c}$ of the polarization size effect. Very approximately, the relation between the screening length λ and shell thickness ΔR determines the length scale of the polarization size effect. Rigorously, the temperature and strain dependences of the critical core radius corresponding to the PE phase instability should be determined from the equation $\alpha^*(T, R_c, \sigma_i) = 0$, where the expression for $\alpha^*(T, R_c, \sigma_i)$ is given by Eq. (6). The size effect of the electrocaloric response is determined by the size effect of the spontaneous polarization P_s, because ΔT_{EC} is proportional to the even powers of P_s in accordance with Eq. (8). That is why the regions of the PE phase and zero ΔT_{EC} coincide in Figs. 5(a) and 5(d), 5(b) and 5(e), and 5(c) and 5(f), respectively.

IV. CONCLUSIONS

This work provides a systematic analytical description of the polar properties of core-shell $BaTiO_3$ nanoparticles using the 2–4–6–8 Landau-Ginzburg-Devonshire free energy functional, which considers nonlinear electrostriction coupling and large Vegard strains in the shell. We revealed that the spontaneous polarization, as high as 50 $\mu C/cm^2$, can be stable in the $BaTiO_3$ core with radius 5–50 nm at room temperature, if a 5-nm paraelectric shell is stretched (3–6)% by the Vegard strains. We can conclude that the nonlinear electrostriction coupling in the core and tensile Vegard strains in the shell are key physical factors of a spontaneous polarization enhancement.

The polarization 50 $\mu C/cm^2$ corresponds to tetragonality ratios as high as 1.02–1.04. The application of higher strains and/or surface stresses would lead to unphysically high tetragonality ratios. In particular, the experimentally observed polarization 130 $\mu C/cm^2$ [6] corresponds to tetragonality ratios as high as 1.27.

The value $\sim$50 $\mu C/cm^2$ is less than half of what is measured experimentally for the spontaneous polarization at room temperature ($\sim$130 $\mu C/cm^2$) for ball-milled core-shell $BaTiO_3$ nanoparticles. A discrepancy of more than a factor of 2 between the considered 2–4–6 and 2–4–6–8 LGD models and experiments [6,11] may be explained by several factors not considered in this work. It can be the dependence of the anisotropic linear electrostriction coefficients Q_{ij} on the preparation method of the nanoparticles, which can be extraordinarily high due to the interface effects [66]. Q_{ij} can reach giant values for milled nanoparticles of 5–10 nm radius and quasi-cubic shape, because evolved surface and corners contribute to the formation of inhomogeneous internal strains. Also, if surface tension coefficient μ at the core-shell interface is negative, the curvature-induced stress ($\sim -\frac{2\mu}{R}$) adds to the tensile Vegard stresses and amplifies the total effect of polarization increase, despite that the negative surface tension could violate the interface equilibrium. Another possibility is a negative extrapolation length in the boundary conditions for polarization, which would support the surface-induced polarization enhancement, despite that the extrapolation length effect is short range [53].

The Vegard strains can improve the electrocaloric properties of a core-shell ferroelectric nanoparticle due to the strain-induced polarization enhancement. In particular, the tensile Vegard strain of (3–6)% increases the spontaneous polarization up to 50 $\mu C/cm^2$, and the spontaneous polarization in turn lowering the EC cooling temperature up to 6 K (in comparison with an unstrained bulk $BaTiO_3$, where the change in the EC temperature cannot exceed 2.5 K). Thus, the dense nanocomposites containing core-shell $BaTiO_3$ nanoparticles can be important for applications as nanocoolers.

ACKNOWLEDGMENTS

The authors are very grateful to the referees for very useful suggestions and stimulating discussion. A.N.M. acknowledges EOARD project 9IOE063 and related STCU partner project P751a. E.A.E. acknowledges the National Academy of Sciences of Ukraine. S.V.K. is supported by the center for 3D Ferroelectric Microelectronics (3DFeM), an Energy Frontier Research Center funded by the U.S. Department of Energy (DOE), Office of Science, Basic Energy Sciences under Award No. DE-SC0021118.

E.A.E. wrote the codes, prepared the figures, and estimated the nonlinear electrostriction couplings. A.N.M. generated the research idea and formulated the electrostatic and elastic problems, performed most of the analytical calculations, and wrote the paper draft. S.V.K. and D.R.E. worked on the results interpretation, discussion, and paper improvement.

[1] T. Mikolajick, S. Slesazeck, H. Mulaosmanovic, M. H. Park, S. Fichtner, P. D. Lomenzo, M. Hoffmann, and U. Schroeder, Next generation ferroelectric materials for semiconductor process integration and their applications, J. Appl. Phys. **129**, 100901 (2021).

[2] K.-H. Kim, I. Karpov, R. H. Olsson III, and D. Jariwala, Wurtzite and fluorite ferroelectric materials for electronic memory, Nat. Nanotechnol. **18**, 422 (2023).

[3] S. Kang, W.-S. Jang, A. N. Morozovska, O. Kwon, Y. Jin, Y.-H. Kim, H. Bae, C. Wang, S.-H. Yang, A. Belianinov, S. Randolph, E. A. Eliseev, L. Collins, Y. Park, S. Jo, M.-H. Jung, K.-J. Go, H. W. Cho, S.-Y. Choi, J. H. Jang, S. Kim, H. Y. Jeong, J. Lee, O. S. Ovchinnikova, J. Heo, S. V. Kalinin, Y.-M. Kim, and Y. Kim, Highly enhanced ferroelectricity in HfO_2-based ferroelectric thin film by light ion bombardment, Science **376**, 731 (2022).

[4] K. P. Kelley, A. N. Morozovska, E. A. Eliseev, V. Sharma, D. E. Yilmaz, A. C. T. van Duin, P. Ganesh, A. Borisevich, S. Jesse, P. Maksymovych, N. Balke, S. V. Kalinin, and R. K. Vasudevan, Oxygen vacancy injection as a pathway to enhancing electromechanical responses in ferroelectrics, Adv. Mater. **34**, 2106426 (2021).

[5] J. Zhu, W. Han, H. Zhang, Z. Yuan, X. Wang, L. Li, and C. Jin, Phase coexistence evolution of nano $BaTiO_3$ as function of particle sizes and temperatures, J. Appl. Phys. **112**, 064110 (2012).

[6] Yu. A. Barnakov, I. U. Idehenre, S. A. Basun, T. A. Tyson, and D. R. Evans, Uncovering the mystery of ferroelectricity in zero dimensional nanoparticles, Nanoscale Adv. **1**, 664 (2019).

[7] H. Zhang, S. Liu, S. Ghose, B. Ravel, I. U. Idehenre, Y. A. Barnakov, S. A. Basun, D. R. Evans, and T. A. Tyson, Structural origin of recovered ferroelectricity in $BaTiO_3$ nanoparticles, Phys. Rev. B **108**, 064106 (2023).

[8] D. A. Freedman, D. Roundy, and T. A. Arias, Elastic effects of vacancies in strontium titanate: Short- and long-range strain fields, elastic dipole tensors, and chemical strain, Phys. Rev. B **80**, 064108 (2009).

[9] Y. Kim, A. S. Disa, T. E. Babakol, and J. D. Brock, Strain screening by mobile oxygen vacancies in $SrTiO_3$, Appl. Phys. Lett. **96**, 251901 (2010).

[10] S. A. Basun and D. R. Evans, Identification of the specific Fe centers and associated defect structure responsible for enhanced dynamic holography in photorefractive $KNbO_3$:Fe, Phys. Rev. B **93**, 094102 (2016).

[11] S. A. Basun, G. Cook, V. Y. Reshetnyak, A. V. Glushchenko, and D. R. Evans, Dipole moment and spontaneous polarization of ferroelectric nanoparticles in a nonpolar fluid suspension, Phys. Rev. B **84**, 024105 (2011).

[12] D. R. Evans, S. A. Basun, G. Cook, I. P. Pinkevych, and V. Yu. Reshetnyak, Electric field interactions and aggregation dynamics of ferroelectric nanoparticles in isotropic fluid suspensions, Phys. Rev. B **84**, 174111 (2011).

[13] G. Cook, A. Glushchenko, V. Yu. Reshetnyak, A. T. Griffith, M. A. Saleh, and D. R. Evans, Nanoparticle doped organic-inorganic hybrid photorefractives, Opt. Express **16**, 4015 (2008).

[14] Y. Reznikov, O. Buchnev, O. Tereshchenko, V. Reshetnyak, A. Glushchenko, and J. West, Ferroelectric nematic suspension, Appl. Phys. Lett. **82**, 1917 (2003).

[15] G. Cook, V. Yu. Reshetnyak, R. F. Ziolo, S. A. Basun, P. P. Banerjee, and D. R. Evans, Asymmetric Freedericksz transitions from symmetric liquid crystal cells doped with harvested ferroelectric nanoparticles, Opt. Express **18**, 17339 (2010).

[16] R. K. Shukla, C. M. Liebig, D. R. Evans, and W. Haase, Electro-optical behavior and dielectric dynamics of harvested ferroelectric $LiNbO_3$ nanoparticles doped ferroelectric liquid crystal nanocolloids, RSC Adv. **4**, 18529 (2014).

[17] E. S. Beh, S. A. Basun, X. Feng, I. U. Idehenre, D. R. Evans, and M. W. Kanan, Molecular catalysis at polarized interfaces created by ferroelectric $BaTiO_3$, Chem. Sci. **8**, 2790 (2017).

[18] H. Atkuri, G. Cook, D. R. Evans, C. I. Cheon, A. Glushchenko, V. Reshetnyak, Yu. Reznikov, J. West, and K. Zhang, Preparation of ferroelectric nanoparticles for their use in liquid crystalline colloids, J. Opt. A: Pure Appl. Opt. **11**, 024006 (2009).

[19] A. Lorenz, N. Zimmermann, S. Kumar, D. R. Evans, G. Cook, and H.-S. Kitzerow, Doping the nematic liquid crystal 5CB with milled $BaTiO_3$ nanoparticles, Phys. Rev. E **86**, 051704 (2012).

[20] D. Caruntu, T. Rostamzadeh, T. Costanzo, S. S. Parizi, and G. Caruntu, Solvothermal synthesis and controlled self-assembly of monodisperse titanium-based perovskite colloidal nanocrystals, Nanoscale **7**, 12955 (2015).

[21] S. Starzonek, S. J. Rzoska, A. Drozd-Rzoska, K. Czupryński, and S. Kralj, Impact of ferroelectric and superparaelectric nanoparticles on phase transitions and dynamics in nematic liquid crystals, Phys. Rev. E **96**, 022705 (2017).

[22] I. U. Idehenre, Yu. A. Barnakov, S. A. Basun, and D. R. Evans, Spectroscopic studies of the effects of mechanochemical synthesis on $BaTiO_3$ nanocolloids prepared using high-energy ball-milling, J. Appl. Phys. **124**, 165501 (2018).

[23] G. Cook, J. L. Barnes, S. A. Basun, D. R. Evans, R. F. Ziolo, A. Ponce, V. Yu. Reshetnyak, A. Glushchenko, and P. P. Banerjee, Harvesting single ferroelectric domain stressed nanoparticles for optical and ferroic applications, J. Appl. Phys. **108**, 064309 (2010).

[24] Yu. Reznikov, in *Liquid Crystals Beyond Displays: Chemistry, Physics, and Applications*, edited by Q. Li (Wiley, New York, 2012), pp. 403–426.

[25] H. Huang, C. Q. Sun, and P. Hing, Surface bond contraction and its effect on the nanometric sized lead zirconate titanate, J. Phys.: Condens. Matter **12**, L127 (2000).

[26] H. Huang, C. Q. Sun, Z. Tianshu, and P. Hing, Grain-size effect on ferroelectric $Pb(Zr_{1-x}Ti_x)O_3$ solid solutions induced by surface bond contraction, Phys. Rev. B **63**, 184112 (2001).

[27] A. N. Morozovska, E. A. Eliseev, and M. D. Glinchuk, Ferroelectricity enhancement in confined nanorods: Direct variational method, Phys. Rev. B. **73**, 214106 (2006).

[28] A. N. Morozovska, M. D. Glinchuk, and E. A. Eliseev, Phase transitions induced by confinement of ferroic nanoparticles, Phys. Rev. B **76**, 014102 (2007).

[29] J. J. Wang, E. A. Eliseev, X. Q. Ma, P. P. Wu, A. N. Morozovska, and Long-Qing Chen, Strain effect on phase transitions of $BaTiO_3$ nanowires, Acta Mater. **59**, 7189 (2011).

[30] A. N. Morozovska, I. S. Golovina, S. V. Lemishko, A. A. Andriiko, S. A. Khainakov, and E. A. Eliseev, Effect of Vegard

strains on the extrinsic size effects in ferroelectric nanoparticles, Phys. Rev. B **90**, 214103 (2014).

[31] A. N. Morozovska and M. D. Glinchuk, Flexo-chemo effect in nanoferroics as a source of critical size disappearance at size-induced phase transitions, J. Appl. Phys. **119**, 094109 (2016).

[32] E. A. Eliseev, A. N. Morozovska, R. Hertel, H. V. Shevliakova, Y. M. Fomichov, V. Yu. Reshetnyak, and D. R. Evans, Flexo-elastic control factors of domain morphology in core-shell ferroelectric nanoparticles: Soft and rigid shells, Acta Mater. **212**, 116889 (2021).

[33] A. Kvasov and A. K. Tagantsev, Role of high-order electromechanical coupling terms in thermodynamics of ferroelectric thin films, Phys. Rev. B **87**, 184101 (2013).

[34] A. N. Morozovska, E. A. Eliseev, A. Ghosh, M. E. Yelisieiev, Y. M. Vysochanskii, and S. V. Kalinin, Anomalous polarization reversal in strained thin films of $CuInP_2S_6$, Phys. Rev. B **108**, 054107 (2023).

[35] A. N. Morozovska, E. A. Eliseev, Y. M. Vysochanskii, V. V. Khist, and D. R. Evans, Screening-induced phase transitions in core-shell ferroic nanoparticles, Phys. Rev. Mater. **6**, 124411 (2022).

[36] A. N. Morozovska, E. A. Eliseev, M. E. Yelisieiev, Y. M. Vysochanskii, and D. R. Evans, Stress-induced transformations of polarization switching in $CuInP_2S_6$ nanoparticles, Phys. Rev. Appl. **19**, 054083 (2023).

[37] Y. L. Wang, A. K. Tagantsev, D. Damjanovic, N. Setter, V. K. Yarmarkin, A. I. Sokolov, and I. A. Lukyanchuk, Landau thermodynamic potential for $BaTiO_3$, J. Appl. Phys. **101**, 104115 (2007).

[38] S. Bourgeois, B. Domenichini, and J. Jupille, Excess electrons at oxide surfaces, in *Defects at Oxide Surfaces*, edited by J. Jupille and G. Thornton, Springer Series in Surface Sciences Vol. 58 (Springer, Cham, 2015), Chap. 4.

[39] M. J. Highland, T. T. Fister, D. D. Fong, P. H. Fuoss, C. Thompson, J. A. Eastman, S. K. Streiffer, and G. B. Stephenson, Equilibrium polarization of ultrathin $PbTiO_3$ with surface compensation controlled by oxygen partial pressure, Phys. Rev. Lett. **107**, 187602 (2011).

[40] G. B. Stephenson and M. J. Highland, Equilibrium and stability of polarization in ultrathin ferroelectric films with ionic surface compensation, Phys. Rev. B **84**, 064107 (2011).

[41] S. M. Yang, A. N. Morozovska, R. Kumar, E. A. Eliseev, Y. Cao, L. Mazet, N. Balke, S. Jesse, R. Vasudevan, C. Dubourdieu, and S. V. Kalinin, Mixed electrochemical-ferroelectric states in nanoscale ferroelectrics, Nat. Phys. **13**, 812 (2017).

[42] A. K. Tagantsev and G. Gerra, Interface-induced phenomena in polarization response of ferroelectric thin films, J. Appl. Phys. **100**, 051607 (2006).

[43] V. A. Shchukin and D. Bimberg, Spontaneous ordering of nanostructures on crystal surfaces, Rev. Mod. Phys. **71**, 1125 (1999).

[44] W. Ma, Surface tension and Curie temperature in ferroelectric nanowires and nanodots, Appl. Phys. A **96**, 915 (2009).

[45] W. Ma, Surface tension and Curie temperature in ferroelectric nanowires and nanodots, Appl. Phys. A **96**, 1035 (2009).

[46] See Supplemental Material at http://link.aps.org/supplemental/10.1103/PhysRevB.109.014104 for a mathematical formulation of the problem, a table of material parameters, a description of methods, and numerical algorithms.

[47] E. A. Eliseev, Y. M. Fomichov, S. V. Kalinin, Y. M. Vysochanskii, P. Maksymovich, and A. N. Morozovska, Labyrinthine domains in ferroelectric nanoparticles: Manifestation of a gradient-induced morphological phase transition, Phys. Rev. B **98**, 054101 (2018).

[48] A. N. Morozovska, E. A. Eliseev, Y. A. Genenko, I. S. Vorotiahin, M. V. Silibin, Ye Cao, Y. Kim, M. D. Glinchuk, and S. V. Kalinin, Flexocoupling impact on the size effects of piezo- response and conductance in mixed-type ferroelectrics-semiconductors under applied pressure, Phys. Rev. B **94**, 174101 (2016).

[49] L. D. Landau and I. M. Khalatnikov, On the anomalous absorption of sound near a second order phase transition point, Dokl. Akad. Nauk SSSR **96**, 469 (1954).

[50] J. Hlinka, Mobility of ferroelectric domain walls in barium titanate, Ferroelectrics **349**, 49 (2007).

[51] Yu. M. Vysochanskii, M. M. Mayor, V. M. Rizak, V. Yu. Slivka, and M. M. Khoma, The tricritical Lifshitz point on the phase diagram of $Sn_2P_2(Se_xS_{1-x})_6$, J. Exp. Theor. Phys. **95**, 1355 (1989).

[52] A. Kohutych, R. Yevych, S. Perechinskii, V. Samulionis, J. Banys, and Yu. Vysochanskii, Sound behavior near the Lifshitz point in proper ferroelectrics, Phys. Rev. B **82**, 054101 (2010).

[53] A. K. Tagantsev, G. Gerra, and N. Setter, Short-range and long-range contributions to the size effect in metal-ferroelectric-metal heterostructures, Phys. Rev. B **77**, 174111 (2008).

[54] C. L. Jia, V. Nagarajan, J. Q. He, L. Houben, T. Zhao, R. Ramesh, K. Urban, and R. Waser, Unit-cell scale mapping of ferroelectricity and tetragonality in epitaxial ultrathin ferroelectric films, Nat. Mater. **6**, 64 (2007).

[55] G. A. Samara, Pressure and temperature dependences of the dielectric properties of the perovskites $BaTiO_3$ and $SrTiO_3$, Phys. Rev. **151**, 378 (1966).

[56] T. Yamada, Electromechanical properties of oxygen octahedra ferroelectric crystals, J. Appl. Phys. **43**, 328 (1972).

[57] D. L. Decker and Y. X. Zhao, Dielectric and polarization measurements on $BaTiO_3$ at high pressures to the tricritical point, Phys. Rev. B **39**, 2432 (1989).

[58] A. J. Bell and L. E. Cross, A phenomenological Gibbs function for $BaTiO_3$ giving correct e field dependence of all ferroelectric phase changes, Ferroelectrics **59**, 197 (1984).

[59] J. J. Wang, P. P. Wu, X. Q. Ma, and L. Q. Chen, Temperature-pressure phase diagram and ferroelectric properties of $BaTiO_3$ single crystal based on a modified Landau potential, J. Appl. Phys. **108**, 114105 (2010).

[60] F. H. Schader, E. Aulbach, K. G. Webber, and G. A. Rossetti, Influence of uniaxial stress on the ferroelectric-to-paraelectric phase change in barium titanate, J. Appl. Phys. **113**, 174103 (2013).

[61] J. Suchanicz, G. Stopa, K. Konieczny, D. Wcislo, M. Dziubaniuk, and J. Rymarczyk, Uniaxial pressure effect on the dielectric properties of the $BaTiO_3$ single crystals, Ferroelectrics **366**, 3 (2008).

[62] S. H. Wemple, M. Didomenico Jr., and I. Camlibel, Dielectric and optical properties of melt-grown $BaTiO_3$, J. Phys. Chem. Solids **29**, 1797 (1968).

[63] W. J. Merz, Double hysteresis loop of $BaTiO_3$ at the Curie point, Phys. Rev. **91**, 513 (1953).

[64] H. D. Megaw, Temperature changes in the crystal structure of barium titanium oxide, Proc. R. Soc. **189**, 261 (1947).

[65] H. F. Kay, Preparation and properties of crystals of barium titanate, $BaTiO_3$, Acta Crystallogr. **1**, 229 (1948).

[66] H. Zhang, N. Pryds, D.-S. Park, N. Gauquelin, S. Santucci, D. V. Christensen, D. Jannis, D. Chezganov, D. A. Rata, A. R. Insinga, I. E. Castelli, J. Verbeeck, I. Lubomirsky, P. Muralt, D. Damjanovic, and V. Esposito, Atomically engineered interfaces yield extraordinary electrostriction, Nature (London) **609**, 695 (2022).

[67] E. A. Eliseev, A. V. Semchenko, Y. M. Fomichov, M. D. Glinchuk, V. V. Sidsky, V. V. Kolos, Yu. M. Pleskachevsky, M. V. Silibin, N. V. Morozovsky, and A. N. Morozovska, Surface and finite size effects impact on the phase diagrams, polar and dielectric properties of (Sr, Bi)Ta_2O_9 ferroelectric nanoparticles, J. Appl. Phys. **119**, 204104 (2016).

[68] The *Mathematica* (https://www.wolfram.com/mathematica) notebook, which contains the codes, is available at https://notebookarchive.org/2023-02-8sdtltx.

[69] K. J. Choi, M. Biegalski, Y. L. Li, A. Sharan, J. Schubert, R. Uecker, P. Reiche, Y. B. Chen, X. Q. Pan, V. Gopalan, and L. Q. Chen, Enhancement of ferroelectricity in strained $BaTiO_3$ thin films, Science **306**, 1005 (2004).

[70] L. D. Landau and E. M. Lifshitz, *Statistical Physics, Course of Theoretical Physics* (Butterworth-Heinemann Pergamon, London, 1984), Vol. 5.

[71] Y. Ishibashi, H. Orihara, and D. R. Tilley, Thickness transitions of ferroelectricity in thin films, J. Phys. Soc. Jpn. **67**, 3292 (1998).

[72] A. N. Morozovska, E. A. Eliseev, M. D. Glinchuk, H. V. Shevliakova, G. S. Svechnikov, M. V. Silibin, A. V. Sysa, A. D. Yaremkevich, N. V. Morozovsky, and V. V. Shvartsman, Analytical description of the size effect on pyroelectric and electrocaloric properties of ferroelectric nanoparticles, Phys. Rev. Mater. **3**, 104414 (2019).

[73] A. N. Morozovska, V. V. Khist, M. D. Glinchuk, V. Gopalan, and E. A. Eliseev, Linear antiferrodistortive-antiferromagnetic effect in multiferroics: Physical manifestations, Phys. Rev. B **92**, 054421 (2015).

[74] F. Jona and G. Shirane, *Ferroelectric Crystals, International Series of Monographs on Solid State Physics* (Pergamon, New York, 1962).